Journal of Photochemistry & Photobiology, B: Biology 205 (2020) 111842

Contents lists available at ScienceDirect

Journal of Photochemistry & Photobiology, B: Biology

journal homepage: www.elsevier.com/locate/jphotobiol

Cr_2O_3/cellulose hybrid nanocomposites with unique properties: Facile synthesis, photocatalytic, bactericidal and antioxidant application

Meng Lu[a], Yongxia Cui[a], Suxia Zhao[b,*], Ali Fakhri[c,d,**]

[a] College of Pharmacy, Henan University of Chinese Medicine, Zhengzhou 450046, China
[b] Third Clinical Medical College, Henan University of Chinese Medicine, Zhengzhou 450008, China
[c] Department of Chemistry, Nano Smart Science Institute, Tehran, Iran
[d] Young Researchers and Elites Club, Science and Research Branch, Islamic Azad University, Tehran, Iran

ARTICLE INFO

Keywords:
Cr_2O_3
Synthesis
Cellulose
Photocatalysis
Biological

ABSTRACT

Development of high responsive photocatalysts for the degradation of dye from water is a significance method to solve the difficulties of water contamination. In the present project, Cr_2O_3 nanoparticles were decorated onto cellulose through a facile synthesis method, which was exposed to characterization by XRD, FESEM, DLS, PL, and UV–vis spectroscopy. The structural attributes confirmed the presence of rhombohedral phase of Cr_2O_3 nanoparticles. The mean crystal size of Cr_2O_3, and Cr_2O_3/cellulose nanocomposites were 38.50 nm, and 50.11 nm, respectively. The band gap values (Eg) of Cr_2O_3, and Cr_2O_3/cellulose nanocomposites were was found 3.00, and 2.53 eV, respectively. Moreover, the morphological and optical studies have been showed the impressive photocatalytic properties of the prepared Cr_2O_3/cellulose nanocomposites. The photocatalytic efficiency of Cr_2O_3, and Cr_2O_3/cellulose nanocomposites has been investigated for the photo-degradation of crystal violet in the ultraviolet light region. The Cr_2O_3/cellulose indicated promising photocatalytic performance and up to 99.65% of the crystal violet was photo-degraded in 40 min. The obtained crystal violet degradation results were fitted onto a Langmuir-Hinshelwood (L-H) plot. The antioxidant performances of Cr_2O_3, and Cr_2O_3/cellulose were analyzed. The beneficial antibacterial performance of the Cr_2O_3/cellulose nanocomposites was tested by various bacteria as *Escherichia coli, Pseudomonas aeruginosa, staphylococcus aurous,* and *Streptococcus pyogenes*.

1. Introduction

The discharge of hazardous and toxic dye compounds from industrial activities into the water is the main problem of environmental contamination, thus damaging the humans and ecosystem due to their toxic properties [1]. The dye compounds are resistant against biodegradation due to their recalcitrant behavior and aromatic structures and produce cancer, diseases, neurotoxicity, and respiratory difficult for humans health [2]. They reduce the sunlight influence into the water source and makes damages to ecosystem life [3]. Therefore, the presence of these dyes from industrial activities should be removed before their release. Nowadays, there is a need to cost-effective water treatment method for removal of dyes. Photocatalysis has showed as an alternative method for the degradation of hazardous and toxic organic compounds [4–9]. In photocatalytic system, the dye photo-degradation reaction is performed in the presence of nano-catalysts under source light irradiation [10]. In recent researches, the several nano semiconductor oxide such as WO_3, TiO_2, Fe_3O_4, and ZnO were used as photocatalyst for degradation of organic compounds [11–14].

Cr_2O_3 is a p-type semiconductor via wide band gap $\approx$ 3.0 eV. Cr_2O_3 has high chemical, thermal stability and eco-friendly properties. It is an important semiconductor oxide that is applied in many technologies as a catalyst [15]. Muzammil Anjum and et al. presented the new Cr_2O_3-C_3N_4 catalyst for photocatalytic activity under visible light irradiation [16]. M.A. Ahmed and et al. investigated the new method for synthesis Cr_2O_3/TiO_2 composites for degradation process [17]. Hadi Salari studies on preparation of Cr_2O_3/Fe_2O_3 nanocomposites for water treatment reaction under visible light irradiation [18].Muhammad Aqeel Ashraf and et al. illustrated the photo-degradation activity of new Cr_2O_3/SiO_2 catalyst for removal of organic compound [19]. Khoirakpam Kesho Singh and et al. analyzed the photochemical activity of Fe_3O_4–Cr_2O_3 nanocomposites and applied in degradation reaction of organochloride compound under ultraviolet irradiation [20].

Cellulose as biological polymer with conjugated structures can be

* Corresponding author at: Third Clinical Medical College, Henan University of Chinese Medicine, Zhengzhou 450008, China.
** Corresponding author at: Department of Chemistry, Nano Smart Science Institute, Tehran, Iran.
E-mail addresses: wsry221@126.com (S. Zhao), Ali.fakhri88@yahoo.com (A. Fakhri).

https://doi.org/10.1016/j.jphotobiol.2020.111842
Received 13 January 2020; Received in revised form 19 February 2020; Accepted 24 February 2020
Available online 27 February 2020
1011-1344/

reduce the band gap and increase the photocatalytic activity [21]. Recent papers have indicated that different metal oxide supported on cellulose for photo-degradation system such as CeO_2/cellulose, ZnO/cellulose, TiO_2/cellulose, and CuO/cellulose nanocomposites [22–26].

Thereupon, the Cr_2O_3/cellulose nanocomposites were synthesized. The morphological and optical properties of the prepared catalysts were characterized. The photocatalytic performance of the Cr_2O_3/cellulose nanocomposites was studied using crystal violet (CV) dye. In addition, the antibacterial and antioxidant performance of Cr_2O_3/cellulose nanocomposites was analyzed.

2. Material and Method

The chemical compounds in this project were procured from Merck Co. with high analytical grade without further treatment.

2.1. Preparation of Cr_2O_3/Cellulose Nanocomposites

50 mL of $CrCl_3.6H_2O$ (0.2 M) was augmented drop by drop in 50 mL NaOH (0.1 M). After that, 30 mL of citric acid solution (0.01 M) was slowly added into the above solution under vigorous stirring at 27 °C. Then, an ultrasonic liquid processors (Hielscher UP-400S; 50/100 Hz) immersed into the mixture solution for 1 h. The suspension was stirred for 2 days at 60 °C. Finally, the product was washed and dried at 130 °C for 5 h. The obtained product was calcined at 650 °C for 3 h.

One gram of cellulose powder was dispersed into 90 mL of sodium metaperiodate solution (0.15 M). The suspension were stirred in the dark at 27 °C. Then, 10 mL of PVP was augmented. The cellulose nanocrystals were freeze-dried and obtained. 0.3 g of Cr_2O_3 and 0.3 g of cellulose were mixed in 60 mL of distilled water and stirred for 40 min. 2.5 mL of CH_3COOH solution was added to prepared suspension and stirred for 60 min. The pH was adjusted to about 7.0 by using potassium hydroxide (0.05 M). The Cr_2O_3/Cellulose was separated and dried at 100 °C for 30 h.

2.2. Characterization Devices

The synthesized catalysts were characterized by X-ray diffraction (XRD), scanning electron microscopy (SEM), energy-dispersive X-ray spectroscopy (EDX), X-ray photoelectron spectroscopy (XPS) and UV–vis spectroscopy. XRD pattern of the composites was recorded on X-ray diffractometer (Philips X'Pert) using Cu Ka radiation. Field emission scanning electron microscopy was performed using Tescan, Japan. UV–visible diffusion spectra was recorded by using Perkin Elmer UV–visible spectrophotometer. The particle size of the composite materials were analyzed by Dynamic light scattering (Nano Series Malvern). Zeta potential of the dilute dispersions (0.1 mg/mL) were performed with a Brookhaven NanoBrook Omni Instrument.

2.3. Photocatalytic Analysis

The photocatalytic activity of Cr_2O_3/Cellulose was studied by degrading the CR dye under UV light illumination. A fixed amount of catalyst (0.1 g/L) was dispersed in 50 mL (10 mg/L) of CR dye solution. The mixture was stirred for 30 min in dark in order to balance reaction. The photo-degradation tests were carried out with UV light source (25 W) and the average intensity was 3.0 mW.cm^{-2}. After light irradiation, 3 mL of the analyte was separated from the reactor and filtered. The residual concentration of CR dye was determined using UV–Vis spectrophotometer (Shimadzu, UV-1900, λ_{max} = 592 nm).

2.4. Antibacterial and Antioxidant Analysis

Examination of the antibacterial properties of the prepared nanomaterials on *Escherichia coli, Pseudomonas aeruginosa, staphylococcus aurous, and Streptococcus pyogenes* by using agar-well diffusion method.

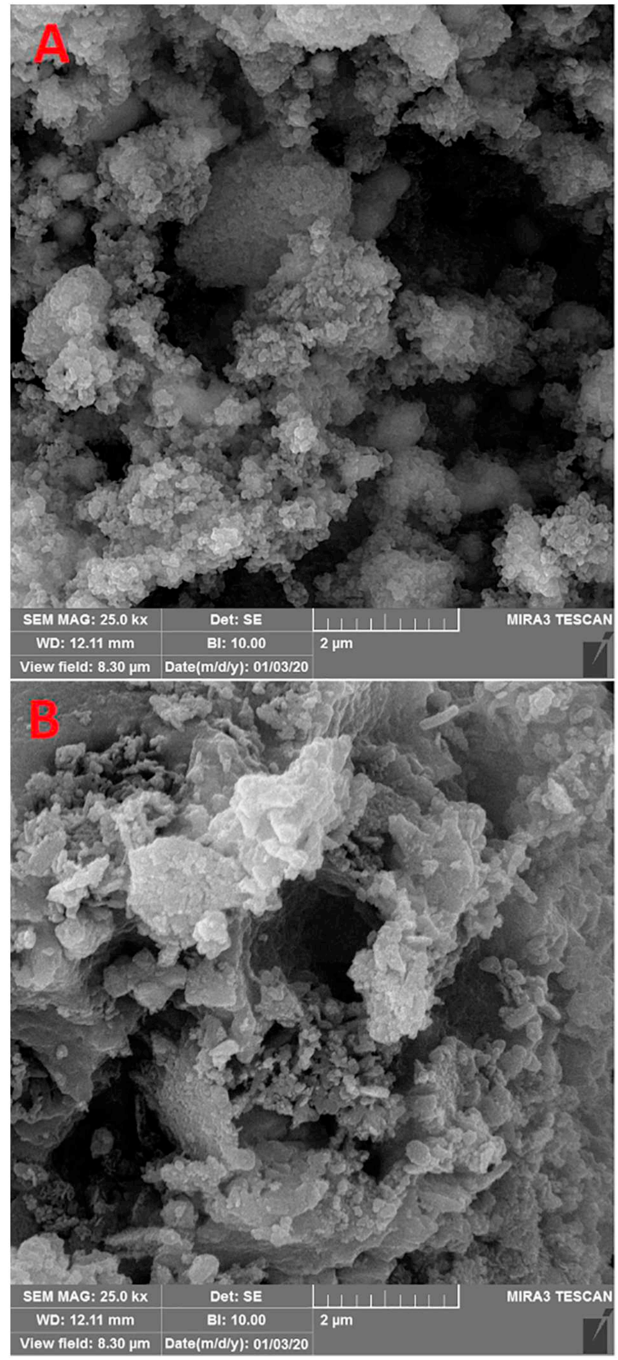

Fig. 1. FESEM images of Cr_2O_3 nanoparticles (A), and Cr_2O_3/Cellulose nanocomposites (B).

Nutrient agar plate's medium was used to this test with 80 μL of 10^6 CFU bacterial suspensions and 40 μL of solution containing the prepared nano-materials (20 mg/mL). These plates were the incubated at 37 °C for 15 h. The inhibition zone diameter was determined for evaluation of antibacterial and antifungal performance.

The antioxidant activity was characterized by using 2,2-diphenyl-2-picrylhydrazyl hydrate method. The solution of DPPH was prepared via methanol. 1 mL of this stock solution was added to 3 mL of the prepared catalyst solution. The mixture was stirred vigorously for 1 h at 27 °C. Then the absorbance value was determined at 520 nm by using a UV–Vis spectrophotometer (Shimadzu, UV-1900).

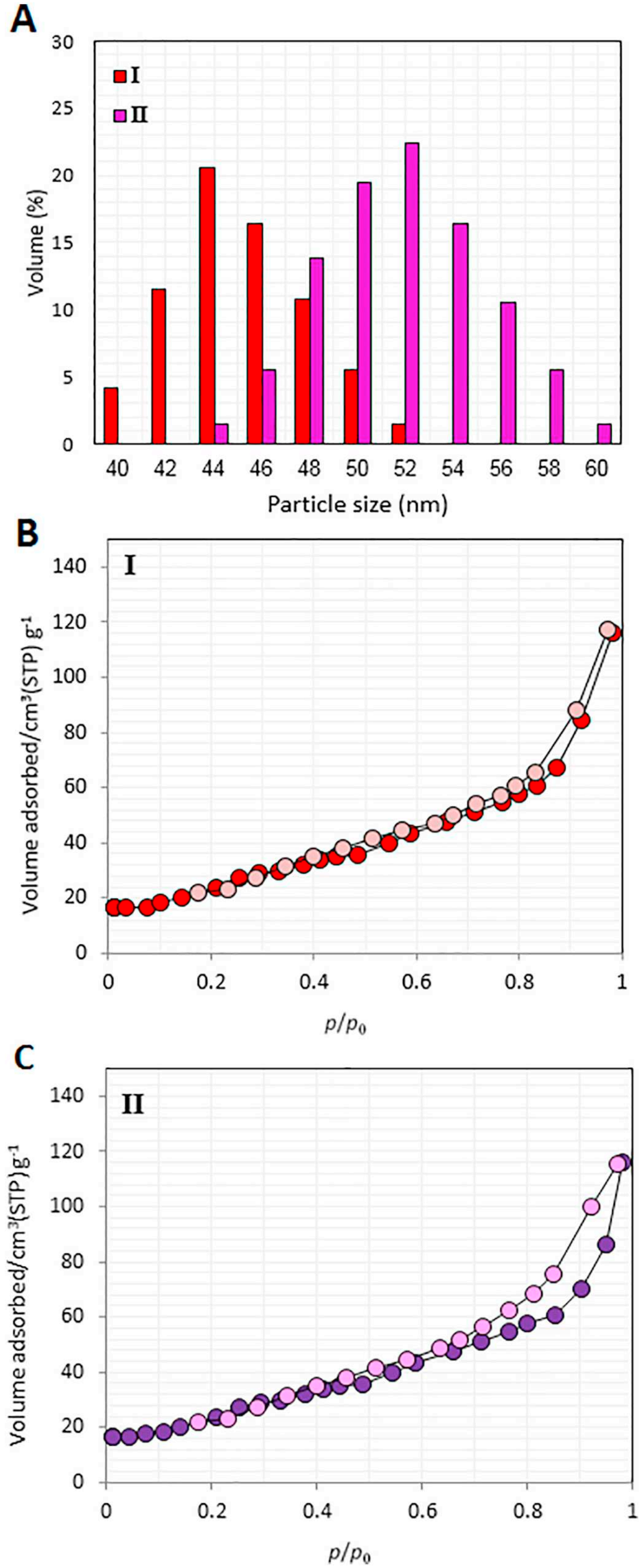

Fig. 2. DLS plot (A), BET plots (B,C) of Cr_2O_3 nanoparticles (I), and Cr_2O_3/Cellulose nanocomposites (II).

3. Results and Discussion

3.1. Characterization of Catalyst

The morphological data of Cr_2O_3 nanoparticles and Cr_2O_3/Cellulose nanocomposites was studied by FESEM (Fig. 1). The pure Cr_2O_3 nanoparticles had a sphere shape morphology with well- distributed and homogeneous nanoparticle sizes. It could be seen FESEM of Cr_2O_3/Cellulose nanocomposites, the Cr_2O_3 nanoparticles could also be well attached to Cellulose, without changing the Cr_2O_3 nanoparticles morphology. The EDX analysis of Cr_2O_3/Cellulose nanocomposites indicated the elemental fraction as Chromium (Cr: 47.07%), Oxygen (O: 39.19%) and Carbon (C: 13.21%). The nanoparticle size distribution of the Cr_2O_3 nanoparticles and Cr_2O_3/Cellulose nanocomposites were determined by dynamic light scattering (DLS) analyzer and indicated in Fig. 2A. The nanoparticle size distribution measured on the basis of percent quantity of different sized value indicated the average size of 44.0 nm and 52.0 nm related to Cr_2O_3 nanoparticles and Cr_2O_3/Cellulose nanocomposites, respectively. The Cr_2O_3 nanoparticles and Cr_2O_3/Cellulose nanocomposites were characterized by Brunauer-Emmett-Teller (BET) method. Outcome indicated that the BET surface area of Cr_2O_3 nanoparticles is 52.19 m^2/g, which illustrated that the Cr_2O_3 nanoparticles has a medium surface area value. Fig. 2B and C indicated the N_2 isotherms of Cr_2O_3/Cellulose nanocomposites. BET surface area of Cr_2O_3/Cellulose nanocomposites is 74.85 m^2/g, which that higher than Cr_2O_3 nanoparticles due to presence of Cellulose in hybrid composites.

Crystallinity properties of Cr_2O_3 nanoparticles and Cr_2O_3/Cellulose nanocomposites were analyzed by X-ray diffraction. Fig. 3 indicates XRD curve of Cr_2O_3 nanoparticles. It indicated the diffraction peaks of Cr_2O_3 crystal at 2θ = 25.6°, 33.1°, 35.9°, 41.8°, 49.7°, 55.5°, 63.1° and 64.8°, with phase plane (012), (110), (104), (113), (024), (116), (214) and (300), related to the rhombohedral phase of Cr_2O_3 (JCPDS no. 38–1479) [20]. Fig. 4A indicates the XRD curve of Cr_2O_3/Cellulose and the diffraction peak was observed at 2θ = 24.2° related to the presence of cellulose in Cr_2O_3/Cellulose nanocomposites. The average crystal size of Cr_2O_3 nanoparticles and Cr_2O_3/Cellulose nanocomposites was calculated with Debye Scherer "$D = k\lambda / \beta(\cos\theta)$" [26–29]. The crystal sizes of Cr_2O_3 nanoparticles and Cr_2O_3/Cellulose nanocomposites were 38.50 nm, and 50.11 nm, respectively.

UV–Visible spectroscopy was studied to evaluate optical properties

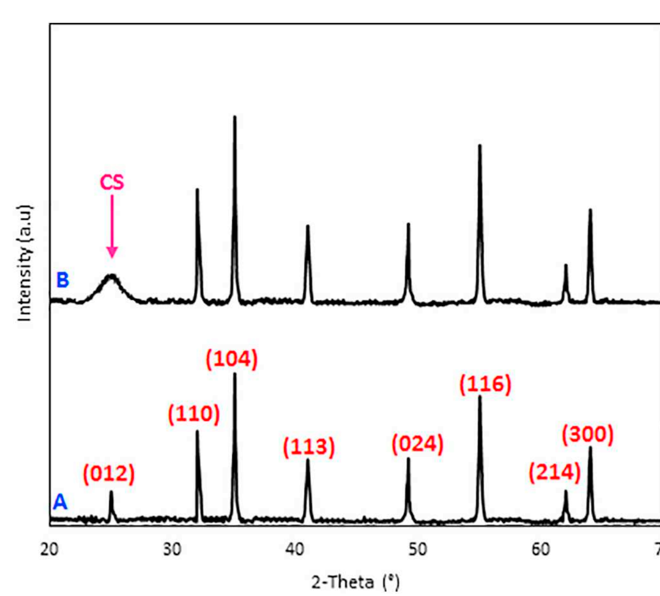

Fig. 3. XRD curves of Cr_2O_3 nanoparticles (A), and Cr_2O_3/Cellulose nanocomposites (B).

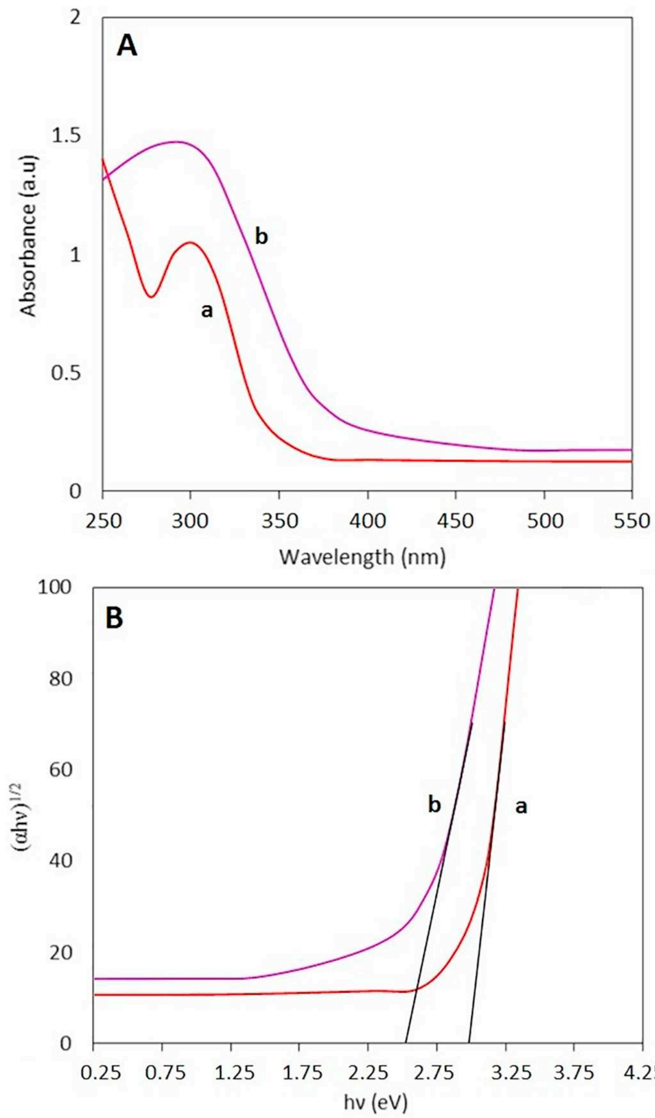

Fig. 4. (A) UV–Vis spectrum, and (B) Kubelka-Munk curve of Cr_2O_3 nanoparticles (a), and Cr_2O_3/Cellulose nanocomposites (b).

of Cr_2O_3 nanoparticles and Cr_2O_3/Cellulose nanocomposites, shown in Fig. 4. The band edge of Cr_2O_3 nanoparticles was observed, and increase to higher wavelength range was found with the addition of Cellulose. A red shift for band gap or the appearance of visible light intensity was addition by the cellulose to metal oxide nanoparticles [30,31]. The absorption spectra shift to a lower energy value with addition of carbon structure can be observed due to the charge-transfer transition between the e^- in the conduction and valence band of Cr_2O_3 [10]. The band gap values (Eg) was found from Kubelka-Munk formula [32] as 3.00 and 2.53 eV for Cr_2O_3 nanoparticles and Cr_2O_3/Cellulose nanocomposites, respectively.

3.2. Photocatalytic Activity

The photocatalytic performance of Cr_2O_3 nanoparticles and Cr_2O_3/Cellulose nanocomposites were studied by degradation of CV under UV light irradiation. The pathways formed in the photo-degradation reaction are toxic and hazardous in environmental [33,34]. Hereupon, the complete photo-degradation is significant for environmental treatment. The change in degradation of CV in the presence of Cr_2O_3 nanoparticles and Cr_2O_3/Cellulose nanocomposites is indicated in Fig. 5A, which reflects the role of photo-catalysts in the degradation of CV. No significance photo-degradation of CV was found in the absence of Cr_2O_3 nanoparticles and Cr_2O_3/Cellulose nanocomposites, illustrating that the prepared catalysts and light are prerequisite for the photo-degradation of CV. The removal of CV by using Cr_2O_3 nanoparticles and Cr_2O_3/Cellulose nanocomposites was found 14.21 and 23.54% under dark medium, respectively. In the presence of Cr_2O_3 nanoparticles and Cr_2O_3/Cellulose nanocomposites, significance degradation was obtained. Compared to pure nanoparticles and hybrid nanocomposites, Cr_2O_3/Cellulose nanocomposites indicated better photo-degradation performance against the removal of CV. It is distinguished that the photocatalytic activity of Cr_2O_3/Cellulose nanocomposites enhances with increasing the time up to 40 min, and the percentage of

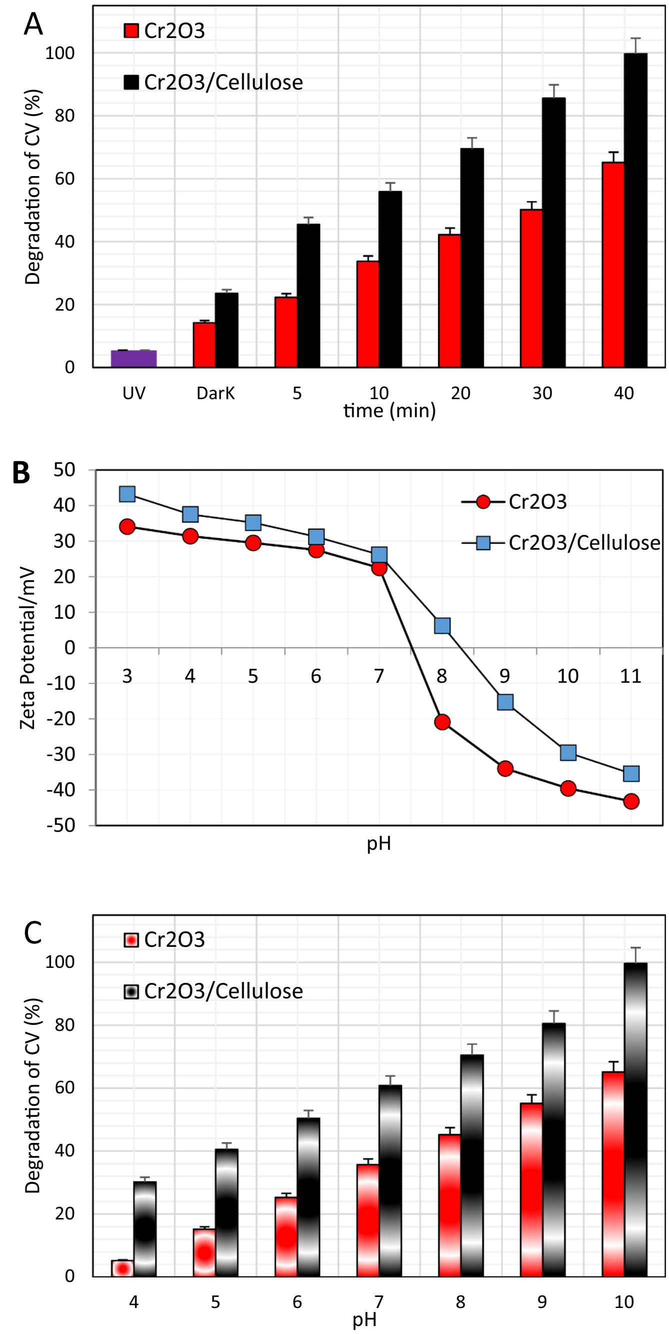

Fig. 5. (A) Photo-degradation of CV under UV light irradiation (pH:10, nano-catalyst dose:0.1 g/L); (B) Zeta potential of prepared catalyst as a function of pH; (C) photo-degradation of CV in different pH (time: 40 min, nano-catalyst dose:0.1 g/L).

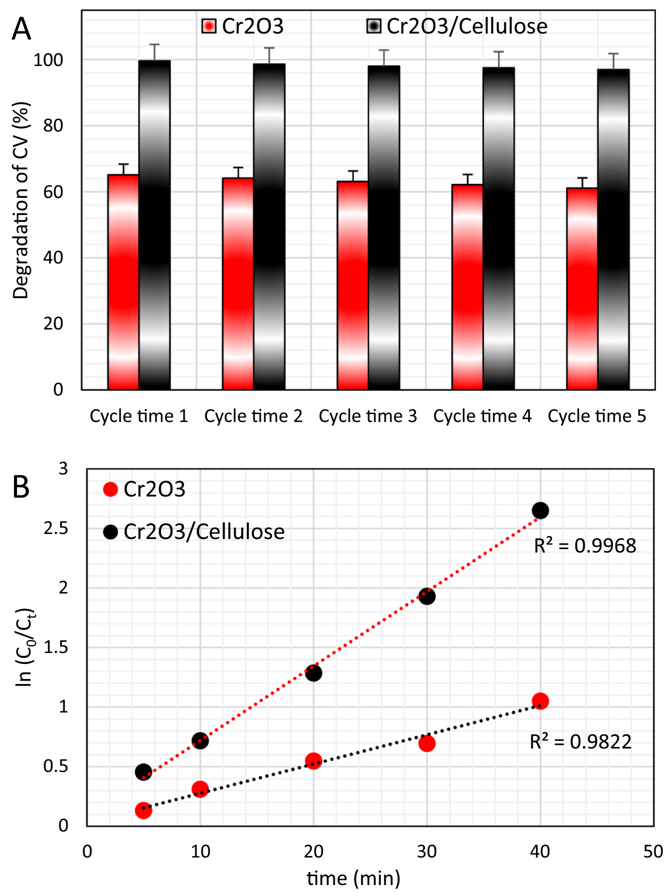

Fig. 6. Plot of nanomaterials behavior in various cycle time of reaction (A), Langmuir-Hinshelwood plot of photocatalytic reaction (B).

photocatalytic activity was 99.65% in during time.

The photocatalytic removal of CV is greatly affected by the solution pH. The surface charge of catalyst, aggregation of catalyst depend on the solution pH and it can influence on catalytic performance [35]. Therefore, the photo-degradation tests were performed at various pH of solution from 4.0 to 10.0. The Zeta potential of Cr_2O_3 nanoparticles and Cr_2O_3/Cellulose nanocomposites was carried out to explain the surface dependent behavior of Cr_2O_3 nanoparticles and Cr_2O_3/Cellulose nanocomposites on the pH medium [10]. The Cr_2O_3 nanoparticles and Cr_2O_3/Cellulose nanocomposites have point of zero charge (pH_{PZC}) at 7.5, and 8.3, respectively (Fig. 5B). At pH values less than pH_{PZC}, catalyst has a positive charge, and, higher pH values, catalyst has a negative charge. The surface charge of crystal violet is positive. Therefore, the optimum pH for high photo-degradation reaction is 10.0 (basic media) (Fig. 5C) [10].

The nano-photocatalyst reusability were important to evaluate catalyst behavior. Cr_2O_3 nanoparticles and Cr_2O_3/Cellulose nanocomposites were washed with several organic and deionized water, after every run, to reuse it for a new run. The photocatalyst stability study was tested for five-time and illustrated in Fig. 6A. The photo-degradation activity of CV was reduced from 99.65% to 97.00% that it's excellent reusability and stability.

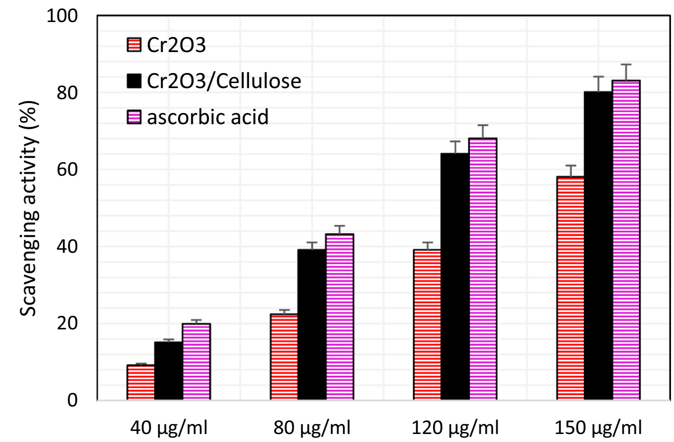

Fig. 7. Antioxidant activity plot of Cr_2O_3 nanoparticles, and Cr_2O_3/Cellulose nanocomposites.

Fig. 6B indicates that the photo-degradation of CV was adjusted to the Langmuir–Hinshelwood analysis by plotting ln (C_o/C_t) versus the time (t) to find regression coefficients value (R^2) [36]. The pseudo-first-order rate constants, k_{app}, were calculated as 0.0245, and 0.0625 min^{-1} for Cr_2O_3 nanoparticles and Cr_2O_3/Cellulose nanocomposites, respectively.

3.3. Antibacterial and Antioxidant Activities

Table 1 illustrates the zone of inhibition of the Cr_2O_3 nanoparticles and Cr_2O_3/Cellulose nanocomposites. Cr_2O_3/Cellulose nanocomposites indicated higher antibacterial behavior versus the bacterial species of *E. coli* (15.13 ± 0.23 mm), *P. aeruginosa* (16.65 ± 0.34 mm), *S. aurous* (22.31 ± 0.31 mm), *and S. pyogenes* (24.00 ± 0.13 mm). Well-diffusion analysis was used to study the antibacterial performance [37–39].

DPPH radical scavenging method was studied for explain of antioxidant behavior of the Cr_2O_3 nanoparticles and Cr_2O_3/Cellulose nanocomposites. The antioxidant performance of prepared nano-materials was distinguished spectrophotometrically. In its radical form, DPPH concentration reduces versus reduction with antioxidant activity. The radical scavenging progress of Cr_2O_3/Cellulose nanocomposites was improved. A significance data was calculated at 150 µg/ml, which is same as the ascorbic acid as control data (Fig. 7) [40,41].

4. Conclusion

In this study, novel catalysts as Cr_2O_3/Cellulose nanocomposites were synthesized through the ultrasound-sol-gel approaches. The structural information of the synthesized catalyst were characterized, and the photocatalytic behavior were studied by degradation of CV dye. XRD curves displayed that all prepared catalyst had great crystallinity. The formation of Cr_2O_3 on cellulose don't change the crystal phase. The maximum CV photo-degradation of 99.65% was found within 40 min of reaction at pH 10, CV concentration of 10 mg/L and photo-catalyst dose of 0.1 g/L under UV irradiation. The bactericidal and antioxidant behavior of the prepared nano-catalyst was investigated and showed that the Cr_2O_3/Cellulose nanocomposites has high bactericidal and antioxidant properties.

Table 1
Diameter of zone of inhibition in (mm) for antibacterial test.

	E. coli	*P. aeruginosa*	*S. aureus*	*S. pyogenes*
Cr_2O_3	8.22 ± 0.05	9.98 ± 0.05	11.75 ± 0.53	13.42 ± 0.28
Cr_2O_3/Cellulose	15.13 ± 0.23	16.65 ± 0.34	22.31 ± 0.31	24.00 ± 0.13

Declaration of Competing Interest

The authors declare that they have no known competing financial interests or personal relationships that could have appeared to influence the work reported in this paper.

Acknowledgements

This project was supported and presented by Nano Smart Science Institute (NSSI), Iran.

References

[1] J.T. Adeleke, T. Theivasanthi, M. Thiruppathi, M. Swaminathan, T. Akomolafe, A.B. Alabi, Photocatalytic degradation of methylene blue by $ZnO/NiFe_2O_4$ nanoparticles, Appl. Surf. Sci. 455 (2018) 195–200.
[2] F.F. Dias, A.A.S. Oliveira, A.P. Arcanjo, F.C.C. Moura, J.G.A. Pacheco, Residuebased iron catalyst for the degradation of textile dye via heterogeneous photo- Fenton, Appl. Catal. B Environ. 186 (2016) 136–142.
[3] L. Zhang, X. Li, M. Wang, Y. He, L. Chai, J. Huang, H. Wang, X. Wu, Y. Lai, Highly flexible and porous nanoparticle-loaded films for dye removal by Graphene oxide–fungus interaction, ACS Appl. Mater. Interfaces 8 (2016) 34638–34647.
[4] F. Zhang, Y. Zhang, G. Zhang, Z. Yang, D.D. Dionysiou, A. Zhu, Exceptional synergistic enhancement of the photocatalytic activity of SnS_2 by coupling with polyaniline and N-doped reduced graphene oxide, Appl. Catal. B Environ. 236 (2018) 53–63.
[5] Y. Zhang, F. Zhang, Z. Yang, H. Xue, D.D. Dionysiou, Development of a new efficient visible-light-driven photocatalyst from SnS_2 and polyvinyl chloride, J. Catal. 344 (2016) 692–700.
[6] Y. Wang, Y. Su, W. Fang, Y. Zhang, SnO_2/SnS_2 nanocomposite anchored on nitrogen-doped RGO for improved photocatalytic reduction of aqueous Cr(VI), Powder Technol. 363 (2020) 337–348.
[7] Y. Zhang, J. Li, H.Y. Xu, One-step in situ solvothermal synthesis of SnS_2/TiO_2 nanocomposites with high performance in visible light-driven photocatalytic reduction of aqueous Cr(VI), Appl. Catal. B Environ. 123–124 (2012) 18–26.
[8] Y. Zhang, L. Yao, G. Zhang, D.D. Dionysiou, One-step hydrothermal synthesis of high-performance visible-light-driven SnS_2/SnO_2 nanoheterojunction photocatalyst for the reduction of aqueous Cr(VI), Appl. Catal. B Environ. 144 (2014) 730–738.
[9] Z. Jiang, K. Chen, Y. Zhang, Y. Wang, Magnetically recoverable $MgFe_2O_4$/conjugated polyvinyl chloride derivative nanocomposite with higher visible-light photocatalytic activity for treating Cr(VI)-polluted water, Sep. Purif. Technol. 236 (2020) 116272.
[10] H. Pan, H. Xie, G. Chen, N. Xu, A. Fakhri, Cr_2S_3-Co_3O_4 on polyethylene glycol-chitosan nanocomposites with enhanced ultraviolet light photocatalysis activity, antibacterial and antioxidant studies, Int. J. Biol. Macromol. 1481 (2020) 608–614.
[11] R. Guo, G. Han, A. Yan, Y. He, T. Yi, Epitaxial growth of metastable phase α-Ag_2MoO_4 on WO_3 surface: visible light-driven photocatalysis, sterilization, and reaction mechanism, J. Alloys Compd. 814 (2020) 152255.
[12] M.R. Al-Mamun, S. Kader, M.S. Islam, M.Z.H. Khan, Photocatalytic activity improvement and application of UV-TiO_2 photocatalysis in textile wastewater treatment, J. Environ. Chem. Eng. 7 (2019) 103248.
[13] S. Huang, J. Zhao, C. Wu, X. Wang, Z. Hu, ZIF-assisted construction of magnetic multiple core-shell Fe_3O_4@ZnO@N-doped carbon composites for effective photocatalysis, Chem. Eng. Sci. 209 (2019) 115185.
[14] Y. Xia, J. Wang, L. Xu, X. Li, S. Huang, A room-temperature methane sensor based on Pd decorated ZnO/rGO hybrids enhanced by visible light photocatalysis, Sensors Actuators B Chem. 304 (2020) 127334.
[15] L. Mei, D. Yan, S. Xie, Z. Lei, X. Ge, Effects of Cr_2O_3 active agent on the weld process dynamic behavior and joint comprehensive properties of fiber laser welded stainless steel thick plate, Opt. Lasers Eng. 128 (2020) 106027.
[16] M. Anjum, R. Kumar, M.A. Barakat, Synthesis of Cr_2O_3/C_3N_4 composite for enhancement of visible light photocatalysis and anaerobic digestion of wastewater sludge, J. Environ. Manag. 212 (2018) 65–76.
[17] M.A. Ahmed, Z.M. Abou-Gamra, A.M. Salem, Photocatalytic degradation of methylene blue dye over novel spherical mesoporous Cr_2O_3/TiO_2 nanoparticles prepared by sol-gel using octadecylamine template, J. Environ. Chem. Eng. 5 (2017) 4251–4261.
[18] H. Salari, Kinetics and mechanism of enhanced photocatalytic activity under visible light irradiation using Cr_2O_3/Fe_2O_3 nanostructure derived from bimetallic metal organic framework, J. Environ. Chem. Eng. 7 (2019) 103092.
[19] M.A. Ashraf, Z. Liu, D. Zheng, C. Li, A. Fakhri, Photocatalytic performance of novel chromium oxide-silicon dioxide decorated on multi-walled carbon nanotubes and graphene oxide nanocomposites: preparation, structural, and optimization, Phys. E. 116 (2020) 113723.
[20] N.K. Kesho Singh, K.K. Senapati, C. Borgohain, K.C., Sarma, newly developed Fe_3O_4–Cr_2O_3 magnetic nanocomposite for photocatalytic decomposition of 4-chlorophenol in water, J. Environ. Sci. 52 (2017) 333–340.
[21] A. Geng, L. Meng, J. Han, Q. Zhong, M. Li, S. Han, C. Mei, L. Xu, L. Tan, L. Gan, Highly efficient visible-light photocatalyst based on cellulose derived carbon nanofiber/BiOBr composites, Cellulose 25 (2018) 4133–4144.
[22] X. He, J. Gan, A. Fakhri, B. Faraji Dizaji, M. Hosseini, Preparation of ceric oxide and cobalt sulfide-ceric oxide/cellulose-chitosan nanocomposites as a novel catalyst for efficient photocatalysis and antimicrobial study, Int. J. Biol. Macromol. 143 (2020) 952–957.
[23] F. Wahid, Y.X. Duan, X.H. Hu, L.Q. Chu, C. Zhong, A facile construction of bacterial cellulose/ZnO nanocomposite films and their photocatalytic and antibacterial properties, Int. J. Biol. Macromol. 132 (2019) 692–700.
[24] Y. Yu, X. Zhu, L. Wang, F. Wu, X. Luo, A simple strategy to design 3-layered au-TiO_2 dual nanoparticles immobilized cellulose membranes with enhanced photocatalytic activity, Carbohydr. Polym. 231 (2020) 115694.
[25] N. Phutanon, K. Motina, Y.-H. Chang, S. Ummartyotin, Development of CuO particles onto bacterial cellulose sheets by forced hydrolysis: a synergistic approach for generating sheets with photocatalytic and antibiofouling properties, Int. J. Biol. Macromol. 136 (2019) 1142–1152.
[26] V.K. Gupta, A. Fakhri, S. Agarwal, E. Ahmadi, P. Afshar Nejad, Synthesis and characterization of MnO_2/NiO nanocomposites for photocatalysis of tetracycline antibiotic and modification with guanidine for carriers of Caffeic acid phenethyl ester-an anticancer drug, J. Photochem. Photobiol. B 174 (2017) 235–242.
[27] Z.B. Zheng, J.J. Sun, A. Fakhri, A. Surendar, A.Z. Ibatova, J.B. Liu, Synthesis, photocatalytic, optical, electronic and biological properties of the CoS_2–CuS on cellulose nanocomposites as novel nano catalyst by a sonochemical, J. Mater. Sci. Mater. Electron. 29 (2018) 18531–18539.
[28] M. Hosseini, N. Fazelian, A. Fakhri, H. Kamyab, S. Chelliapan, Preparation, and structural of new NiS-SiO_2 and Cr_2S_3-TiO_2 nano-catalyst: Photocatalytic and antimicrobial studies, J. Photochem. Photobiol. B 194 (2019) 128–134.
[29] A. Fakhri, S. Tahami, P.A. Nejad, Preparation and characterization of Fe_3O_4-Ag_2O quantum dots decorated cellulose nanofibers as a carrier of anticancer drugs for skin cancer, J. Photochem. Photobiol. B 175 (2017) 83–88.
[30] Z. Luo, Q.H. Gao, Decrease in the photoactivity of TiO_2 pigment on doping with transition metals, J. Photochem. Photobiol. A Chem. 63 (2003) 367–375.
[31] R. Casarano, L.C. Fidale, C.M. Lucheti, T. Heinze, O.A. El Seoud, Expedient, accurate methods for the determination of the degree of substitution of cellulose carboxylic esters: application of UV–vis spectroscopy (dye solvatochromism) and FTIR, Carbohydr. Polym. 83 (2011) 1285–1292.
[32] S. Habibi, M. Jamshidi, Synthesis of TiO_2 nanoparticles coated on cellulose nanofibers with different morphologies: effect of the template and sol-gel parameters, Mater. Sci. Semicond. Process. 109 (2020) 104927.
[33] I. Bibi, S. Kamal, A. Ahmed, M. Iqbal, S. Nouren, K. Jilani, N. Nazar, M. Amir, A. Abbas, S. Ata, F. Majid, Nickel nanoparticle synthesis using camellia Sinensis as reducing and capping agent: growth mechanism and photo-catalytic activity evaluation, Int. J. Biol. Macromol. 103 (2017) 783–790.
[34] B. Yu, B. Yang, G. Li, H. Cong, Preparation of monodisperse cross-linked poly (glycidyl methacrylate)@Fe_3O_4@diazoresin magnetic microspheres with dye removal property, J. Mater. Sci. 53 (2018) 6471–6481.
[35] M.N. Chong, B. Jin, C.W.K. Chow, C. Saint, Recent developments in photocatalytic water treatment technology: a review, Water Res. 44 (2010) 2997–3027.
[36] X. Li, T. Wan, J. Qiu, H. Wei, X. Tan, In-situ photocalorimetry-fluorescence spectroscopy studies of RhB photocatalysis over Z-scheme g-C_3N_4@ag@Ag_3PO_4 nanocomposites: a pseudo-zero-order rather than a first-order process, Appl. Catal. B Environ. 217 (2017) 591–602.
[37] J. Alimunnisa, K. Ravichandran, K.S. Meena, Synthesis and characterization of ag@SiO_2 core-shell nanoparticles for antibacterial and environmental applications, J. Mol. Liq. 231 (2017) 281–287.
[38] K. Akhil, J. Jayakumar, G. Gayathri, S. Sudheer Khan, Effect of various capping agents on photocatalytic, antibacterial and antibiofilm activities of ZnO nanoparticles, J. Photochem. Photobiol. B 160 (2016) 32–42.
[39] K. Akhil, S. Sudheer Khan, Effect of humic acid on the toxicity of bare and capped ZnO nanoparticles on bacteria, algal and crustacean systems, J. Photochem. Photobiol. B 167 (2017) 136–149.
[40] S. Kato, D. Matsuoka, N. Miwa, Antioxidant activities of nano-bubble hydrogen dissolved water assessed by ESR and 2,2′-bipyridyl methods, Mater. Sci. Eng. C 53 (2015) 7–10.
[41] Akeem Babatunde Dauda, Abdullateef Ajadi, Adenike Susan Tola-Fabunmi, Ayoola Olusegun Akinwole, Waste production in aquaculture: Sources, components and managements in different culture systems, Aquaculture and Fisheries 4 (3) (2019) 81–88.